Influence of substrate surface polarity on homoepitaxial growth of ZnO layers by chemical vapor deposition

Markus R. Wagner,* Til P. Bartel, Ronny Kirste, and Axel Hoffmann
Institute of Solid State Physics, TU Berlin, Hardenbergstrasse 36, 10623 Berlin, Germany

Joachim Sann, Stefan Lautenschläger, and Bruno K. Meyer
I. Physics Institute, Justus Liebig University, Heinrich-Buff-Ring 16, 35592 Giessen, Germany

C. Kisielowski
National Center for Electron Microscopy, Materials Sciences Division, Lawrence Berkeley National Laboratory, 1 Cyclotron Road, Berkeley, California 94720, USA

(Received 6 June 2008; revised manuscript received 17 October 2008; published 9 January 2009)

The influence of the substrate polarity (Zn polar or O polar) on the structural and optical properties of homoepitaxial ZnO epilayers grown by chemical vapor deposition is investigated. The polarity of the epilayer is controlled by the substrate polarity as shown by high-resolution transmission electron microscopy (TEM) imaging. Changes in stoichiometry in the epilayer are studied by quantitative TEM analysis. A small compressive strain of $\epsilon_{cc}=3\times10^{-4}$ is observed in both epilayers and x-ray diffraction measurements indicate a superior structural quality of the epilayers compared to the substrate. Cross-sectional Raman spectroscopy also demonstrates the superior quality of the epilayers, although high strain is present within the substrates. The phonon deformation-potential parameters of the strain sensitive E_2(high) Raman mode are determined to $a=-730$ cm^{-1} and $b=-1000$ cm^{-1}. Differences in the excitonic luminescence including the appearance of different emission lines and an increased full width at half maximum in O-face epilayers are observed. It is suggested that the impurity diffusion from the substrate to the layer is affected by the substrate surface polarity with lower impurity concentrations in the Zn-polar film compared to the O-polar epilayer.

DOI: 10.1103/PhysRevB.79.035307 PACS number(s): 78.30.Fs, 68.37.Og, 68.35.Fx, 71.55.Gs

I. INTRODUCTION

The fabrication of efficient optoelectronic devices based on ZnO depends on the structural perfection and optical properties of the epilayers. Homoepitaxial growth of ZnO has the great potential to provide high-quality epilayers without strain or dislocations induced by the mismatch of lattice or thermal-expansion coefficients. A lower dislocation density and the absence of a defective substrate-layer interface are promising prospects. Due to their wurtzite structure, ZnO substrates can be Zn polar (0001) or O polar $(000\bar{1})$ along $\langle 0001\rangle$. The two faces have different compositions and surface configurations leading to variations in the chemical and physical properties.[1–4] Other wurtzite semiconductors, such as GaN, show similar dependencies on the surface polarity, which influences the diffusion process of impurities, defect incorporation, and dislocation formation. Consequently, the incorporation of shallow acceptors for *p*-type conductivity substantially depends on the polarity of the surface.[5,6] This is best proven by the successful fabrication of *p*-conductive GaN:Mg on Ga-polar substrates, while N-polar GaN shows hexagonal hillocks, high resistivity, and no *p*-type conduction.[7,8]

Since ZnO has the same crystal structure and similar material parameters as GaN, Zn-polar faces are likely to possess more favorable properties toward *p*-conductive ZnO. This is supported by the first reports of successful *p*-type doping on Zn-polar ZnO.[9,10] Nevertheless, only few publications report on the impact of surface polarity on structural and optical properties using homoepitaxy.[1,3,4,11] The fact that many ZnO layers also show rather large variation in the c/a lattice-constant ratio, ranging between 1.6018 and 1.6035, can also be correlated with the impurity concentration and polarity of the substrate.[12–14] It could be observed that, for example, the large concentration of Li in ZnO substrates by Tokyo Denpa leads to rather tensile strain in the layers. This is probably caused by the smaller ionic radius of Li (0.59 Å) substituted for Zn (0.60 Å).[15] On the other hand, the diffusion and incorporation of defects for homoepitaxy on Crystec substrate usually results in compressively strained layers. The current understanding of the impact of surface polarity on these issues is still very fragmentary.

In this paper, we study the influence of the substrate polarity on the structural and optical properties of homoepitaxially grown ZnO epilayers. First, the influence of the substrate polarity on the polarity of the epilayer is studied. Then, the effect of impurities and their correlation to local strain fields in the epilayers and substrates are evaluated. Finally, bound exciton transitions for the different surface polarities are identified and the deformation potential for the E_2(high) Raman mode is determined.

II. EXPERIMENT

Nominally undoped ZnO layers of approximately 1.2 μm in thickness were grown by chemical vapor deposition on Zn- and O-polar ZnO substrates. The epilayers were grown simultaneously in the same reactor to ensure direct comparability between the samples. Before growth the substrates were annealed at 1150 °C in a flowing oxygen atmosphere.

This procedure removes polishing damages and produces terracelike structures which are necessary for two-dimensional growth.

For structural analysis high-resolution transmission electron microscopy (HRTEM) and x-ray diffraction (XRD) were performed. For HRTEM the samples were prepared according to standard cross-sectional preparation procedure with mechanical thinning and ion milling. After ion milling the samples were etched by a KOH solution to produce clean and atomically flat sample wedges. Micrographs were recorded on the OÅM based on a Phillips CM300 FEG operated at 300 kV. This machine has an information limit of 0.8 Å. That corresponds to the usable resolution when a holographic method (exit wave reconstruction by through focal series[16]) is used to correct for aberrations up to the spherical aberration. As the phase of the exit wave is dependent on the atomic number Z of atoms in the sample, it can be used for the chemical identification of single atom columns. The XRD data were acquired using a Philips X'pert Pro materials research diffractometer (MRD) employing the Cu $K\alpha_1$ radiation with a four-crystal monochromator set for the (220) Ge reflection mode in the primary beam.

Photoluminescence (PL) measurements were performed using a 325 nm HeCd laser with 45 mW as excitation source. The laser beam hits the samples at an arbitrary angle between **k** and the principal axis of the crystals **c**. The emitted light was detected by a bialkali photomultiplier in combination with a Spex 1 m double spectrometer. Micro-Raman spectra were excited using an argon-krypton-ion laser, which was focused by micro-optics to a radial symmetric spot of about 500 nm in diameter. The Raman signal was recorded using a Dilor XY 800 triple-grating Raman spectrometer with 1800 lines/mm and a liquid-nitrogen-cooled charge-coupled device (CCD) camera as detector. The scattered light was detected in backscattering geometry.

III. STRUCTURAL ANALYSIS

ZnO is a wurtzite crystal with hexagonal bilayers of Zn and O in the (0001) plane. The polarity of such a crystal is defined by the type of atom in the top half of this bilayer with respect to the growth direction. In Zn-polar (Zn-face) material, zinc atoms lie in the top half of the bilayer, whereas in O-polar (O-face) ZnO, oxygen is in the top layer. Electron affinities and chemical properties strongly depend on the polarity of the material. Hence, the polarity is an important parameter of epitaxial growth.

The polarity can be determined in real space by HRTEM imaging of Zn and O columns which are separately resolved and identified in the bilayers. In projection, the Zn-O dumbbell is largest in $[11\bar{2}0]$ zone axis where it is 1.12 Å wide. Resolving the dumbbell is complicated by the large atomic number difference of zinc (Z=30) and oxygen (Z=8). The large and heavy Zn columns localize the electron wave strongly and induce a large phase shift that makes Zn columns appear strong but small in-phase images. The O columns next to them appear large but smeared out and can be difficult to resolve. Only if the dumbbell is successfully resolved, zinc and O columns can be identified and allow a direct determination of the material's polarity.

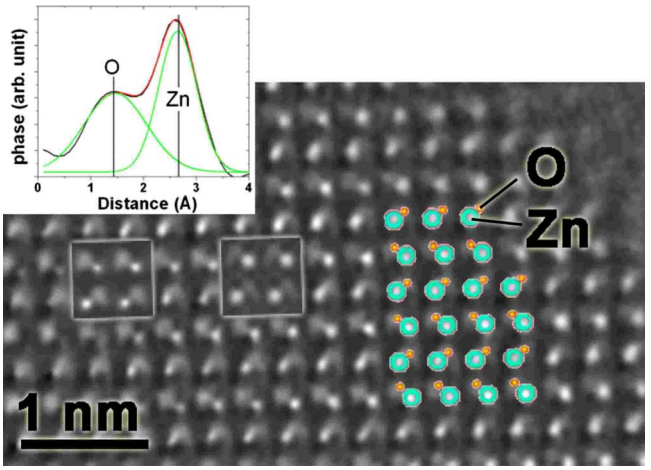

FIG. 1. (Color online) Phase of the reconstructed exit wave of a ZnO substrate. The sample gets thicker from right to left. An atomic overlay shows the $[11\bar{2}0]$ zone axis of ZnO as used for image simulations. The simulations are compared with the experiment for two thicknesses (squares). The inset shows a line profile over the Zn-O dumbbell.

For illustration, Fig. 1 shows the phase of the reconstructed exit wave of a wedge-shaped ZnO substrate in $[11\bar{2}0]$ orientation. An atomic overlay sketches the Zn and O columns in this orientation (rings for zinc; small dots for O columns). Using this atomic model, exit wave simulations were computed for 3 and 6 nm thicknesses and overlaid to the image. The contrast of the simulations was adjusted to the experiment because of Stobbs factor.[17] With this correction, the simulations agree very nicely with the reconstructed exit wave. As seen in the inset, Zn and O columns are easily discernible and the polarity of the material can thus be determined on a microscopic level by HRTEM.

In a next step, the polarities in the studied samples are investigated. Figure 2 shows the phases of the reconstructed exit waves in the substrates and epilayers of the O-face and Zn-face samples. Again, an overlay sketches the Zn and O columns. It is seen that the polarity of the epilayers is the same as in the substrate. Reconstructions were undertaken in various locations of the epilayers and always showed the same polarity.

Inversion domains as they are sometimes observed in GaN (Ref. 18) were detected neither by HRTEM nor by dark field TEM imaging. It is thus concluded that in the studied samples, the polarity of the homoepitaxially grown epilayers is solely controlled by the polarity of the substrates.

For a quantitative analysis the phases from Fig. 2 are compared to simulations. A discrepancy of the experimental values to the simulations could indicate a change in stoichiometry. If, for example, the experimentally measured phase in the O column is higher then predicted by theory, one or more heavy atoms must be present in that column. Of course this necessitates an accurate reconstruction and determination of the sample thickness. For comparison with the experiment a through-focal series of a wedge-shaped $Zn_{0.5}O_{0.5}$ sample oriented along the in $[11\bar{2}0]$ zone axis was simulated

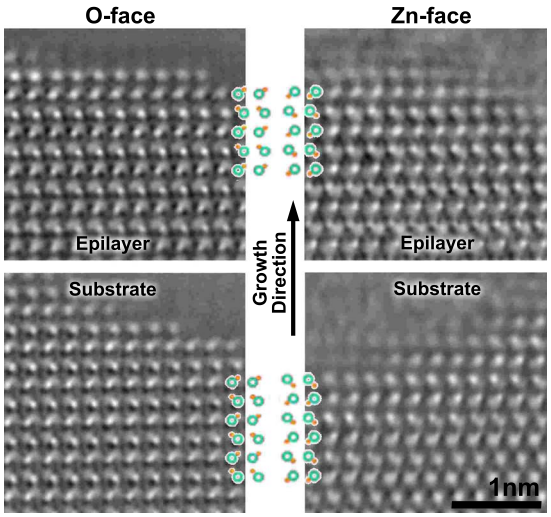

FIG. 2. (Color online) Phase of the exit waves of substrate and epilayer of the O-face (left) and Zn-face (right) samples. The overlay sketches the atoms in $[11\bar{2}0]$ zone axis. Again rings represent Zn columns; dots represent O columns. The polarity of the epilayers is the same as in the substrate.

using the MACTEMPAS software package and settings corresponding to the OÅM.[19] Image contrast was adapted to match the recorded micrographs by the addition of a gray level value (Stobbs factor). Then, an exit wave was reconstructed from the simulated image series. Note that the simulations are not sensitive to changes in polarity since the crystal structure remains the same.

In the experimental images, a nonisoplanicity across the field of view, in this case a change in focus due to a tilted exit surface, was corrected by adjusting the defocus. The thickness was experimentally determined by the use of background gray level oscillations (for more details, see Ref. 20).

The phase was extracted by linescans over the Zn-O dumbbell. The maxima were Gaussian fitted for every column as shown in the inset of Fig. 1. The height of the Gaussian fit was used to quantify the phase shift. The same procedure was applied for the simulated and experimental phase images. The resulting phase shifts in the respective atomic columns are shown in Fig. 3 as a function of thickness (straight lines are from the simulations, thin lines with data points are from the experiment). The quantitative agreement of the simulations and the experiment is reasonable, confirming the correct identification of the Zn and O columns. For the O columns in the O-polar epilayer a reduced phase shift is observed, while in the Zn-polar sample the shift is increased. Under the presumption that the reconstruction and the thickness determination are accurate, it could be concluded that oxygen vacancies are present in the O-face material and heavy atoms (such as Zn or dopants) are present in the Zn-face material on oxygen sites.

Unfortunately several factors hamper this interpretation. Changes in stoichiometry could also be present in the Zn columns which would lead to an inaccurate determination of the thickness and makes the interpretation of phase effects more difficult. Further, it is seen that in some cases the experimental phase in the Zn columns scatters and can be significantly lower than that predicted by theory. This is attributed to a slight sample tilt or an incorrect exit wave reconstruction due to wrong aberration parameters. Despite these obstacles, the presented images provide a useful polarity determination at a microscopic level and an outlook on the power of phase analysis in HRTEM. Since the phase of the exit wave carries all chemical information with subangstrom spatial resolution, it allows the direct measurement of stoichiometric changes in the sample. It is only a matter of sensitivity and resolution whether it can be recovered with sufficient accuracy. The TEAM microscope is being developed with the goal of quantitative TEM at an atomic level[21] and it is expected to be of great help to study the nonstoichiometry and defect distribution in materials such as ZnO.

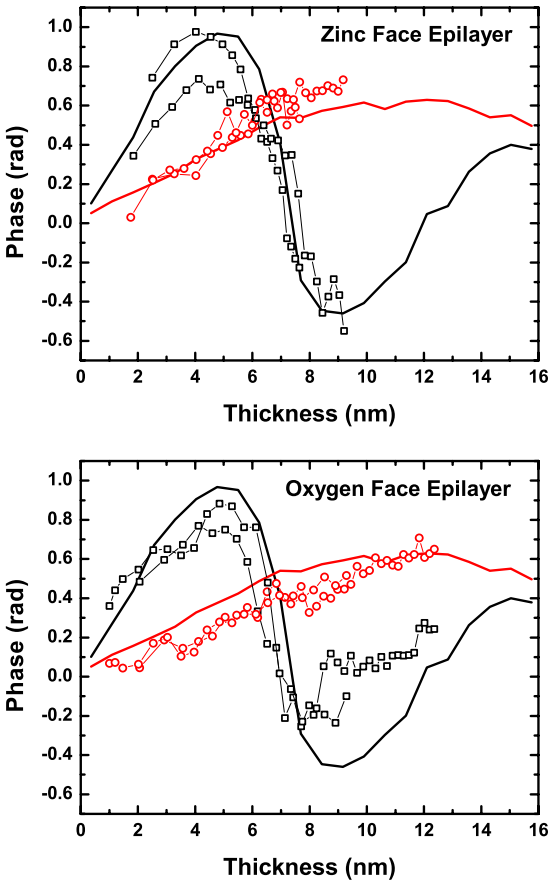

FIG. 3. (Color online) Phase of Zn and O columns in the epilayer of the Zn-face (upper graph) and O-face (lower graph) samples. Thin lines with data points represent experimental data; straight lines result from simulations.

Finally, the crystal quality of the samples was studied by XRD measurements. A ω-2θ scan of the (0002) and (0004) peaks revealed no separate diffraction peaks for both epilayers and the substrate (not shown). Considering the resolution of the instrument, we estimate the maximum strain along the c axis to $\epsilon_{cc} < 3 \times 10^{-4}$. The full width at half maximum (FWHM) of the (0002) peak is determined to 17.5″ in the Zn-face layer and 18″ in the O-face layer compared to 27″ in the substrate. These results demonstrate the superior structural quality of both epilayers in comparison to the substrate and a negligible impact of the substrate polarity on the XRD data.

IV. DEFECT-INDUCED STRAIN DISTRIBUTION

In order to determine the strain in the epilayers from low-temperature PL spectra, we first focus merely on the free exciton transitions. The possible symmetry of the exciton states is determined by the symmetry of the conduction and valence bands. The conduction band in ZnO has Γ_7 symmetry while the valence band is split due to crystal-field interaction and spin-orbit coupling into three subbands, whereby two bands have Γ_7 symmetry and one has Γ_9 symmetry. Therefore, the following exciton symmetries are possible:

$$\Gamma_7^c \otimes \Gamma_7^v = \Gamma_1 \oplus \Gamma_2 \oplus \Gamma_5 \tag{1}$$

$$\Gamma_7^c \otimes \Gamma_9^v = \Gamma_5 \oplus \Gamma_6. \tag{2}$$

The ordering of the valence bands was extensively discussed in literature since the first publications in the early 1960s. In this work, we follow the original designation of Thomas and Hopfield.[22] Consequently, the visible *A* excitons have Γ_1 and Γ_5 symmetries (the Γ_2 exciton is a pure triplet state with a total spin of $S=1$ which is dipole forbidden). Since dipole-allowed exciton states interact with the eigenvalues of the electromagnetic field, exciton polaritons are formed which lead to a longitudinal-transverse splitting of the Γ_5 state. The excitation of the longitudinal exciton polariton by the transverse electromagnetic wave can be observed due to structural imperfections for $\mathbf{k} \| \mathbf{c}$ or for arbitrary angles between $\mathbf{k}$ and $\mathbf{c}$ as used in our setup. In the Zn-face sample, three transitions in the range of the free *A* exciton are present. The longitudinal and transversal *A* exciton polaritons are observed at $E[A_L(\Gamma_5)]=3.377\ 36$ eV and $E[A_T(\Gamma_5)]=3.376\ 06$ eV, whereas the 3.375 29 eV transition originates from the $A_L(\Gamma_1)$ exciton (see Sec. V). The size of the *L*-*T* splitting of the Γ_5 *A* exciton polariton is 1.3 meV but differs in dependence of the investigated samples as demonstrated by the large variation in reported values in the literature. The observed splitting is similar compared to the *L*-*T* splitting published by Hopfield and Thomas[23] (1.2 meV), Wrzesinski[24] (1.42 meV), Chichibu *et al.*[25] (1.5 meV), and Kurtze *et al.*[26] (1.5 meV), but is significantly smaller compared to the splitting published by Blattner *et al.*[27] (2.2 meV), Teke *et al.*[28] (2.6 meV), and Reynolds *et al.*[29] (3.6 meV). Additionally, there is also a significant variation in the absolute energetic position of the free excitons. Aside from the assignment of different peaks to the same transition in the literature, different effects including strain, piezoelectric fields, and variations in the lattice constants may contribute to the energetic variations.

In the investigated Zn-face sample, the energies of the Γ_5 *A* exciton polaritons at 3.377 36 and 3.376 06 eV exhibit a blueshift of 160 μeV compared to the Γ_5 *A* exciton-polariton transitions in the substrate at 3.377 20 and 3.375 90 eV. This shift of the *A* free excitons to higher energies can be related to the presence of uniaxial tensile strain along the *c* axis ϵ_{cc}, i.e., biaxial compressive strain in the *a* plane.[30] The excitonic shift is approximated by evaluating the strain Hamiltonian including first- and second-order terms.[31] It is given by

$$E(X_A) = E_A^0 + (D_1 - D_2/\mu)\epsilon_{cc} + a_+(D_3 - D_4/\mu)\epsilon_{cc} - a_+a_-[(D_3 - D_4/\mu)\epsilon_{cc}]^2(E_C^0 - E_A^0)^{-1}, \tag{3}$$

where $2a_\pm = 1 \pm [\Delta_1 - \Delta_2][(\Delta_1 - \Delta_2)^2 + 8\Delta_2^2]^{-1/2}$, with the deformation potentials D_i, the crystal-field and spin-orbit splitting parameters Δ_1 and Δ_2, the Poisson ration $\mu = C_{13}/C_{33}$, and the elastic moduli C_{ij}. $E_A^0 = 3.3759$ eV and $E_C^0 = 3.4199$ eV are the energies of the free *A* and *C* excitons in unstrained ZnO, respectively. Using values for the deformation potentials and splitting parameters of $D_1 = -3.90$ eV, $D_2 = -4.13$ eV, $D_3 = -1.15$ eV, $D_4 = 1.22$ eV, $\Delta_1 = 38.3$, and $\Delta_2 = 2.1$ (Ref. 32) and average values for the elastic constants of $C_{13} = 105.6$ and $C_{33} = 210.2$,[33,34] we calculate the strain for the Zn-face sample to be $\epsilon_{cc} = 2.1 \times 10^{-4}$ along the *c* axis and $\epsilon_{aa} = -5.2 \times 10^{-5}$ in the *a* plane. A similar calculation for the O-face sample is complicated by the much weaker and broadened free exciton luminescence. However, the position of the bound exciton transitions with their well-known localization energies[35] suggests a somewhat larger blueshift of approximately 250 μeV. This corresponds to strain values of $\epsilon_{cc} = 3.3 \times 10^{-4}$ and $\epsilon_{aa} = -8.2 \times 10^{-5}$ in the O-polar sample.

The weaker free exciton emission in the O-face sample can be explained by an increased impurity concentration, which leads to an efficient localization of free excitons at impurities and the formation of bound excitons. The increased impurity concentration in the O-face epilayers is confirmed by recently published results of secondary-ion mass spectroscopy (SIMS).[36] It is shown that the impurity concentration in the investigated samples is significantly higher in the O-face samples. This is most pronounced for the alkali metals (Li, Na, and K), which concentrations are up to 2 orders of magnitude higher compared to the Zn-face samples. Since O-face and Zn-face samples were always grown simultaneously in the same reactor chamber, the incorporation of different amounts of impurities by contaminations during the growth can be excluded. Consequently, it is suggested that the incorporation of impurity atoms from the substrate into the epilayer is facilitated for the O-polar surface. The larger impurity concentration in the O-face sample correlates with an increased FWHM of all bound exciton lines with values of $\Gamma_{BX} \geq 120$ μeV. This interpretation is further supported by the higher strain in the O-face sample since impurities with their different ionic radii are expected to increase local strain fields.

The formation of local strain is studied as a function of depth for both surface polarities. For this purpose cross-sectional (in-plane) micro-Raman measurements in $x(yy)\bar{x}$ configuration were performed. The $x(yy)\bar{x}$ geometry in the case of in-plane and the $z(..)\bar{z}$ geometry in the case of on-plane measurements are selected to probe the strain properties. Therefore, the position of the E_2(high) mode is analyzed since it is, other than the TO and LO vibration modes, nonpolar and is not affected by free carriers or internal electric fields but only by strain. Raman selection rules show that the A_1(TO), E_2(low), and E_2(high) modes are the only Raman-allowed modes for wurtzite ZnO in $x(yy)\bar{x}$ scattering geometry.[37] The depth-dependent shift of the E_2(high)

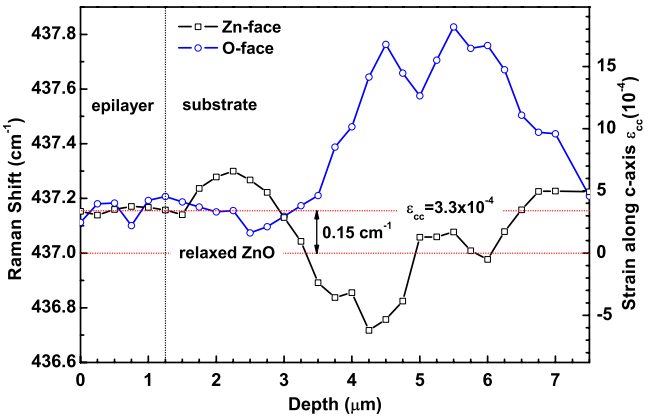

FIG. 4. (Color online) Depth-dependent shift of the E_2(high) mode in cross-sectional micro-Raman measurements. Circles and squares indicate the peak position in O-face- and Zn-face-terminated samples at room temperature.

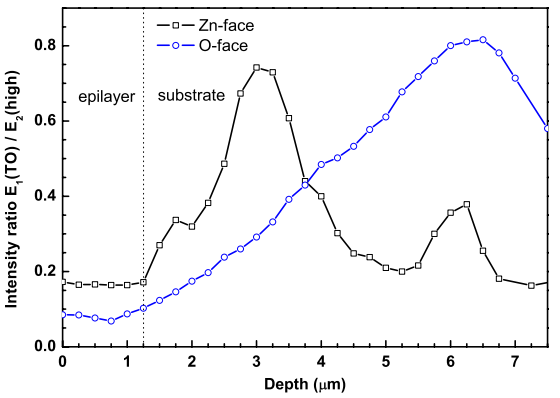

FIG. 5. (Color online) Depth-resolved intensity ratio of the E_1(TO) to E_2(high) Raman modes for Zn-face and O-face ZnO at a depth of 0–7 μm.

optical-phonon mode at room temperature is displayed in Fig. 4. The E_2(high) value is steady in the epilayer with small fluctuations of 0.1 cm^{-1} in the O-face sample. In contrast to the small variations in the epilayers, changes of up to 0.8 cm^{-1} in the top 6 μm of the substrate are observed. The ability to grow high-quality epilayers on substrates with inhomogeneous strain distribution by homoepitaxy is clearly demonstrated by these measurements in agreement with the XRD data. Still, the variations in the O-polar epilayer suggest that larger localized strain fields can be present due to a higher impurity concentration.

The magnitude of the strain-induced shift of the phonon mode $\Delta\Omega_{E_2(\mathrm{high})}=2a\epsilon_{aa}+b\epsilon_{cc}$ is determined by the phonon deformation-potential parameters a and b which are specific for each phonon mode. Based on the previously determined strain [Eq. (3)], we evaluate the strain-induced Raman shift in order to derive the specific deformation potentials for the E_2(high). With the relation $\epsilon_{cc}=-2(C_{13}/C_{33})\epsilon_{aa}$ the following equation can be derived:

$$\Delta\Omega_{E_2(\mathrm{high})}=[b-a(C_{33}/C_{13})]\epsilon_{cc}. \quad (4)$$

The phonon frequency shift at hydrostatic compression of a hexagonal crystal is characterized by the Grüneisen parameter

$$\gamma=-\frac{2a(C_{33}-C_{13})+b(C_{11}+C_{12}-2C_{13})}{\Omega(C_{11}+C_{12}+2C_{33}-4C_{13})}, \quad (5)$$

as a function of the deformation-potential parameters. The two independent equations enable the calculation of a and b. We use average values for the Grüneisen parameter $\gamma=1.89$ (Refs. 38–40) and the elastic constants $C_{11}=208.4$, $C_{12}=119.4$, $C_{13}=105.6$, and $C_{33}=210.2$.[33,34] The average position of the E_2(high) Raman mode in the epilayers is determined to 437.15 cm^{-1}. This corresponds to a strain-induced shift of $\Delta E_2(\mathrm{high})=0.15$ cm^{-1} with respect to 437.0 cm^{-1} in strain-free ZnO single crystals.[37] We calculate the phonon deformation-potential constants a and b for the E_2(high) mode to $a=-730$ cm^{-1} and $b=-1000$ cm^{-1}. The error in these values is mainly determined by the uncertainty in the literature for the Grüneisen parameter and is estimated to be of around 10%. These values are in good agreement with the results published by Gruber *et al.*[41]

Aside from the strain evaluation, micro-Raman measurements are used to investigate crystal imperfections in the substrates and epilayers. Figure 5 shows the intensity ratio of the E_1(TO) to E_2(high) Raman modes measured in the $x(yy)\bar{x}$ configuration. In this geometry the E_2(low), E_2(high), and A_1(TO) Raman modes are allowed. However, the E_1(TO) mode is only allowed in the $x(yz)\bar{x}$ configuration where the E_2(high) is forbidden. For clarity, only the first 7.5 μm is displayed with a spacial resolution of 250 nm. In the epilayer, the intensity ratio in both samples is small and of constant value as expected by the Raman selection rules with slightly higher variations in the O-face sample. On the contrary, the substrate shows regions with non-perfect-crystal symmetry or orientation where the forbidden E_1(TO) appears with an intensity of up to 80% compared to the allowed E_2(high) mode. Possible explanations for the appearance of a forbidden Raman mode are weakened selection rules due to crystal perturbations, multireflections, or a tilting of the c axis. Such a tilting would lead to a changed geometry, consequently resulting in different selection rules. Hence, previously forbidden Raman modes could appear. These variations in the orientation of c axis can be measured by ion channeling measurements or XRD in different reflections.[42] However, we found no evidence for a tilting of the c axis in our XRD measurements. Crystal perturbations, such as defect clusters or inhomogeneous doping profiles due to impurity diffusion, may also lead to a local relaxation of selection rules in Raman scattering. Although it is not possible to draw a final conclusion on the effects involved in the lowering or changing of the symmetry, the intensity ratio and strain evaluation of the Raman modes and the XRD data show the superior quality of the grown epilayers even on non-perfect-crystal structures.[43]

V. OPTICAL PROPERTIES

Figure 6 displays the low-temperature luminescence of epilayers grown on Zn-face- and O-face-terminated substrate

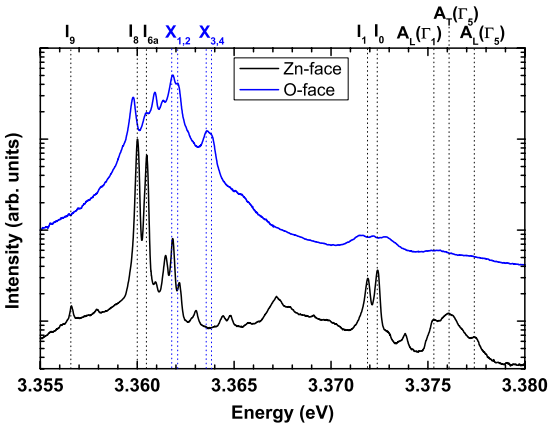

FIG. 6. (Color online) PL spectra of homoepitaxial grown ZnO layers on Zn- and O-face substrate surfaces; (T=1.6 K).

in the range of the free and bound exciton transitions. Apparently, there are different excitonic recombinations depending on the surface polarity of the ZnO substrate. This is reproducible for various Zn-face and O-face samples.

The luminescence spectrum of the Zn-face grown sample is dominated by the I_{6a} (Al) and I_8 (Ga) neutral-donor bound exciton lines.[35] These are accompanied by the ionized donors I_0 and I_1 which form correlated pairs with the I_{6a} and I_8 excitons, respectively.[44] Apart from the weak I_9 exciton (In donor), the sample exhibits several narrow transition lines with a FWHM as small as 80 μeV. Finally, the previously discussed exciton polaritons of the A valence band are clearly observed.

By contrast, the bound exciton spectrum of the O-face sample is dominated by the I_8, I_{6a}, I_6, and I_5 transition lines between 3.359 78 and 3.361 37 eV. Additionally, we observe two luminescence structures $X_{1,2}$ and $X_{3,4}$ consisting each of two transition lines at 3.361 85 eV (X_1), 3.362 15 eV (X_2), 3.363 65 eV (X_3), and 3.363 95 eV (X_4). The energetic distance of 0.3 meV between X_1 to X_2 is the same as those of X_3 to X_4. The line splitting of X_1 to X_3 and X_2 to X_4 is 1.8 meV. Temperature-dependent measurements further show a thermalization behavior, which can be explained by a defect complex with energy splittings of 0.3 and 1.8 meV in the ground state and excited state, respectively.[36] Consequently, these four transitions are attributed to the same defect complex. A possible candidate for this defect is a Zn interstitial-acceptor pair which behaves as shallow donor complex.[45] It should be noted that the transition lines of this defect complex could not be observed in any sample grown on Zn-polar substrate. Although the Zn-face sample exhibits narrow peaks at similar energies compared to the $X_{1,2}$ lines, these transitions do probably not originate from the same defect complex. This conclusion is supported by the strong correlation between the $X_{1,2}$ and $X_{3,4}$ lines concerning intensity ratio, energetic distance, thermalization and decay constants, which is not given in the Zn-face samples. Particularly, the Zn-face sample shows neither any peaks at the energy of X_3 and X_4 nor a constant intensity ratio of X_1 to X_2 as observed in the O-face samples. The peaks at 3.3628 and 3.3614 eV are well known in the literature and are usually labeled I_4 and I_5, respectively.[35] The origin and chemical identity of the other weak lines in the Zn-face sample remains uncertain.

VI. CONCLUSION

In conclusion, we presented results of structural and optical characterizations of homoepitaxially grown ZnO epilayers on Zn- and O-terminated ZnO substrates. HRTEM confirmed that the polarity of the epilayer is controlled by the polarity of the substrate. The identification of the atomic columns could be confirmed by a good agreement of the phases of the reconstructed exit waves with theoretical simulations. However, the quantitative analysis of the phases for stoichiometric determination is still limited by noise in microscopes without hardware aberration correction. XRD measurements show that the quality of the epilayers is improved for both polarities compared to the substrate.

The impact of different surface polarities is most pronounced in the excitonic luminescence spectra. Linewidths of bound excitons are as low as 80 μeV in the Zn face and 120 μeV in the O-face material. A reduced full width at half maximum of exciton lines, a smaller shift of the free exciton, and less intense impurity related recombination lines in Zn-face epilayer indicate a better quality compared to the O-face specimens. Micro-Raman measurements demonstrate that both surface polarities lead to a reduction in strain in the epilayer with slightly higher variations in the Raman shift in the O-face sample. The residual strain along the c axis was found to be very small with $\epsilon_{cc}=2.1\times10^{-4}$. The E_2(high) phonon deformation-potential parameters were determined to $a=-730$ cm^{-1} and $b=-1000$ cm^{-1}. In conclusion, the ability to grow high-quality epilayers with very small residual strain (even on inferior substrates) was demonstrated by XRD and micro-Raman measurements. It is suggested that growth on Zn-polar substrates results in lower impurity concentrations and better optical properties of the epilayer compared to O-face crystals.

ACKNOWLEDGMENTS

Parts of this work were supported by the DFG within Grants No. SFB 296 and No. SFB 787. M.R.W. acknowledges the Ernst-von-Siemens Foundation for support. T.P.B. acknowledges the German National Academic Foundation for support. HRTEM was conducted at NCEM supported by DOE under Contract No. DE-AC02-05CH11231.

*markus.wagner@tu-berlin.de

[1] R. E. Sherriff, D. C. Reynolds, D. C. Look, B. Jogai, J. E. Hoelscher, T. C. Collins, G. Cantwell, and W. C. Harsch, J. Appl. Phys. **88**, 3454 (2000).
[2] B. Meyer and D. Marx, Phys. Rev. B **67**, 035403 (2003).
[3] H. Matsui, H. Saeki, T. Kawai, A. Sasaki, M. Yoshimoto, M. Tsubaki, and H. Tabata, J. Vac. Sci. Technol. B **22**, 2454 (2004).
[4] H. Xu, K. Ohtani, M. Yamao, and H. Ohno, Appl. Phys. Lett. **89**, 071918 (2006).
[5] M. Sumiya, K. Yoshiumra, K. Ohtsuka, and S. Fuke, Appl. Phys. Lett. **76**, 2098 (2000).
[6] F. Tuomisto, K. Saarinen, B. Lucznik, I. Grzegory, H. Teisseyre, T. Suski, S. Porowski, P. R. Hageman, and J. Likonen, Appl. Phys. Lett. **86**, 031915 (2005).
[7] L. K. Li, M. J. Jurkovic, W. I. Wang, J. M. V. Hove, and P. P. Chow, Appl. Phys. Lett. **76**, 1740 (2000).
[8] A. J. Ptak, T. H. Myers, L. T. Romano, C. G. V. de Walle, and J. E. Northrup, Appl. Phys. Lett. **78**, 285 (2001).
[9] D. C. Look, D. C. Reynolds, C. W. Litton, R. L. Jones, D. B. Eason, and G. Cantwell, Appl. Phys. Lett. **81**, 1830 (2002).
[10] X.-L. Guo, J.-H. Choi, H. Tabata, and T. Kawai, Jpn. J. Appl. Phys., Part 2 **40**, L177 (2001).
[11] S. A. Chevtchenko, J. C. Moore, Ü. Özgür, X. Gu, A. A. Baski, H. Morkoç, B. Nemeth, and J. E. Nause, Appl. Phys. Lett. **89**, 182111 (2006).
[12] H. Karzel *et al.*, Phys. Rev. B **53**, 11425 (1996).
[13] S. Desgreniers, Phys. Rev. B **58**, 14102 (1998).
[14] Ü. Özgür, Y. I. Alivov, C. Liu, A. Teke, M. A. Reshchikov, S. Dogan, V. Avrutin, S.-J. Cho, and H. Morkoc, J. Appl. Phys. **98**, 041301 (2005).
[15] R. D. Shannon, Acta Crystallogr., Sect. A: Cryst. Phys., Diffr., Theor. Gen. Crystallogr. **32**, 751 (1976).
[16] C. Kübel and A. Thust, in NATO Science Series II: Mathematics, Physics and Chemistry (Springer Netherlands, 2006), Vol. 211, pp. 373–392.
[17] A. Howie, Ultramicroscopy **98**, 73 (2004).
[18] T. V. Shubina *et al.*, Phys. Rev. B **67**, 195310 (2003).
[19] R. Kilaas, MACTEMPAS, 2007 (http://www.totalresolution.com).
[20] T. P. Bartel, Ph.D. thesis, Technical University of Berlin (2008).
[21] http://ncem.lbl.gov/TEAM project/
[22] J. J. Hopfield, J. Phys. Chem. Solids **15**, 97 (1960).
[23] J. J. Hopfield and D. G. Thomas, Phys. Rev. Lett. **15**, 22 (1965).
[24] J. Wrzesinski, Ph.D. thesis, University Dortmund, Germany, 1997.
[25] S. F. Chichibu, T. Sota, G. Cantwell, D. B. Eason, and C. W. Litton, J. Appl. Phys. **93**, 756 (2003).
[26] G. Kurtze, W. Maier, K. Kempf, G. Schmieder, H. Schrey, C. Klingshirn, B. Hönerlage, and U. Rössler, in Proceedings of the 15th International Conference on the Physics of Semiconductors, Kyoto 1980 [J. Phys. Soc. Jpn. **49**, Suppl. A, 559 (1980)].
[27] G. Blattner, G. Kurtze, G. Schmieder, and C. Klingshirn, Phys. Rev. B **25**, 7413 (1982).
[28] A. Teke, Ü. Özgür, S. Dogan, X. Gu, H. Morkoc, B. Nemeth, J. Nause, and H. O. Everitt, Phys. Rev. B **70**, 195207 (2004).
[29] D. C. Reynolds, D. C. Look, B. Jogai, and T. C. Collins, Appl. Phys. Lett. **79**, 3794 (2001).
[30] B. Gil, A. Lusson, V. Sallet, S.-A. Said-Hassani, R. Triboulet, and P. Bigenwald, Jpn. J. Appl. Phys., Part 2 **40**, L1089 (2001).
[31] J. Rowe, M. Cardona, and F. Pollak, Solid State Commun. **6**, 239 (1968).
[32] J. Wrzesinski and D. Frohlich, Phys. Rev. B **56**, 13087 (1997).
[33] B. Bateman, J. Appl. Phys. **33**, 3309 (1962).
[34] I. B. Kobiakov, Solid State Commun. **35**, 305 (1980).
[35] B. K. Meyer *et al.*, Phys. Status Solidi B **241**, 231 (2004).
[36] S. Lautenschlaeger, J. Sann, N. Volbers, B. K. Meyer, A. Hoffmann, U. Haboeck, and M. R. Wagner, Phys. Rev. B **77**, 144108 (2008).
[37] T. C. Damen, S. P. S. Porto, and B. Tell, Phys. Rev. **142**, 570 (1966).
[38] S. S. Mitra, O. Brafman, W. B. Daniels, and R. K. Crawford, Phys. Rev. **186**, 942 (1969).
[39] F. Decremps, J. Pellicer-Porres, A. M. Saitta, J.-C. Chervin, and A. Polian, Phys. Rev. B **65**, 092101 (2002).
[40] J. Serrano, A. H. Romero, F. J. Manjon, R. Lauck, M. Cardona, and A. Rubio, Phys. Rev. B **69**, 094306 (2004).
[41] T. Gruber, G. M. Prinz, R. Kling, F. Reuss, W. Limmer, and A. Waag, J. Appl. Phys. **96**, 289 (2004).
[42] V. Ratnikov, R. Kyutt, T. Shubina, T. Paskova, E. Valcheva, and B. Monemar, J. Appl. Phys. **88**, 6252 (2000).
[43] M. R. Wagner, U. Haboeck, P. Zimmer, A. Hoffmann, S. Lautenschläger, C. Neumann, J. Sann, and B. Meyer, Proc. SPIE **6474**, 64740X (2007).
[44] B. K. Meyer, J. Sann, S. Lautenschläger, M. R. Wagner, and A. Hoffmann, Phys. Rev. B **76**, 184120 (2007).
[45] D. C. Look, G. C. Farlow, P. Reunchan, S. Limpijumnong, S. B. Zhang, and K. Nordlund, Phys. Rev. Lett. **95**, 225502 (2005).